SCIENCE CHINA
Physics, Mechanics & Astronomy

• Article •

October 2012 Vol.55 No.10: 1863–1872
doi: 10.1007/s11433-012-4887-2

Tomographic TR-PIV measurement of coherent structure spatial topology utilizing an improved quadrant splitting method

YANG ShaoQiong[1] & JIANG Nan[1,2,3*]

[1] *Department of Mechanics, School of Mechanical Engineering, Tianjin University, Tianjin 300072, China;*
[2] *State Key Laboratory of Non-linear Mechanics, Institute of Mechanics, Chinese Academy of Sciences, Beijing 100080, China;*
[3] *Tianjin Key Laboratory of Modern Engineering Mechanics, Tianjin 300072, China*

Received November 18, 2011; accepted June 13, 2012; published online August 23, 2012

In this paper, we calculated the spatial local-averaged velocity strains along the streamwise direction at four spatial scales according to the concept of spatial local-averaged velocity structure function by using the three-dimensional three-component database of time series of velocity vector field in the turbulent boundary layer measured by tomographic time-resolved particle image velocimetry. An improved quadrant splitting method, based on the spatial local-averaged velocity strains together with a new conditional sampling phase average technique, was introduced as a criterion to detect the coherent structure topology. Furthermore, we used them to detect and extract the spatial topologies of fluctuating velocity and fluctuating vorticity whose center is a strong second-quadrant event (Q2) or a fourth-quadrant event (Q4). Results illustrate that a closer similarity of the multi-scale coherent structures is present in the wall-normal direction, compared to the one in the other two directions. The relationship among such topological coherent structures and Reynolds stress bursting events, as well as the fluctuating vorticity was discussed. When other burst events are surveyed (the first-quadrant event Q1 and the third-quadrant event Q3), a fascinating bursting period circularly occurs: Q4-S-Q2-Q3-Q2-Q1-Q4-S-Q2-Q3-Q2-Q1 in the center of such topological structures along the streamwise direction. In addition, the probability of the Q2 bursting event occurrence is slightly higher than that of the Q4 event occurrence. The spatial instable singularity that almost simultaneously appears together with typical Q2 or Q4 events has been observed, which is the main character of the mutual induction mechanism and vortex auto-generation mechanism explaining how the turbulence is produced and maintained.

turbulent boundary layer, coherent structure, burst, TR-PIV, Q2/Q4, local-averaged velocity strain, quadrant splitting method

PACS number(s): 47.27.Jv, 47.27.N, 47.27.De, 47.20.Bp, 47.80.Cb, 47.11.St, 61.25.-f

Citation: Yang S Q, Jiang N. Tomographic TR-PIV measurement of coherent structure spatial topology utilizing an improved quadrant splitting method. Sci China-Phys Mech Astron, 2012, 55: 1863−1872, doi: 10.1007/s11433-012-4887-2

1 Introduction

Since 1967 when Kline et al. [1] observed the low/high-speed streaks and the burst events in the flat-plate turbulent boundary layer (TBL), the conventional understanding of mechanism of wall turbulence, which was considered as fully random motions of fluid particles, has completely changed. Existing research results show that within the TBLs we can clearly observe the repeatability [2] of a variety of similar processes as well as the extended self-similarity [3] of multi-scale eddy structures, which are called coherence. The coherence, namely, coherent motion in wall turbulent flow is commonly associated with eddy structure [2,4,5]. Moreover, vortices are the key elements in many models for wall-bounded turbulence [6,7]. The observable vortices usually behave as streamwise vortices and hairpin

*Corresponding author (email: nanj@tju.edu.cn)

vortices, where the latter are used as a general term to denote horseshoe, arch, cane and hairpins. It is the model that has been developed for more than two decades, in which the structures of the TBL consist of quasi-streamwise vortices near the wall, a hierarchy of hairpin vortex packets extending through the logarithmic layer [8], large-scale motions having streamwise extent of the order of the thickness of the TBL, and very-large-scale motions being much longer than the boundary layer thickness [9]. They are collectively called coherent structures, which play a significant role in momentum, energy and mass transforming, as well as in producing and maintaining turbulence.

Burst as a name for a single event has been dropped from the vocabulary in favor of the term bursting process (or simply the old term burst) to cover the complete sequence of events [10], such as spatially self-organized ejection and sweep events, which are defined respectively as the transport of low momentum fluid away from the wall and the transport of high momentum fluid towards the wall [11]. According to the previous quadrant splitting method [12,13], ejections and sweeps are also well known as Q2 and Q4 events respectively, which yields the most important contributions to the Reynolds shear stress. Such events have been found in the three-dimensional three-component (3D-3C) time-resolved particle image velocimetry (TR-PIV) data of Schröder et al. [14], but they could not be confirmed yet as an essential mechanism for the TBLs. Similarly, other burst events, the first-quadrant event (Q1) and the third-quadrant event (Q3), which will be illustrated later, are also defined in the four quadrants of the fluctuation velocity components in streamwise-wall normal ($u'-w'$) plane. In this present paper, we have detected that a complete bursting process typically contains four quadrant events just as that defined above, using an improved quadrant splitting method (IQSM) which will be formulated clearly in sect. 2. Furthermore, the interesting relationship among such coherent structures and bursting events, as well as the fluctuating vorticity will be discussed in sect. 3.

2 Experiments and methods

2.1 Experimental set-up and basic flow field

The experiments have been performed in the water tunnel at TU Delft where a turbulent boundary layer basic flow has been established along a vertically mounted flat acrylic glass plate at a free-stream velocity of 530 mm/s. The dimensions of the plate with an elliptic leading edge are 2500 mm×800 mm (Length×Width). The flow on the observation side was tripped by a spanwise attached zig-zag band 150 mm downstream of the leading edge (see schematic diagram in Figure 1), and a nearly zero pressure gradient was achieved by adjusting a trailing-edge flap. The light was introduced parallel to the plate and perpendicular to the mean flow direction. The sufficient light was scattered by the polyamide seeding particles with 56 μm mean diameters. The temperature during the measurement was kept constant, while the turbulence level of the free-stream velocity was below 0.5%.

In order to estimate the general characterization of the TBL flow, the first step is that a focal length f=105 mm lens from Nikon was used for a high-resolution 2C-PIV measurement with a low-repetition rate system composed of a Big Sky CFR-200 laser delivering 200 mJ/pulse energy and a LaVision Imager PRO-X camera with a 4M pixel sensor. The resulting semi-logarithmic boundary layer profile scaled with wall units (WU) and basic fluid flow properties of the TBL are respectively given in Figure 2 and Table 1. Here Re_θ is the Reynolds number based on momentum thickness and free-stream velocity. The friction Reynolds number $\mathrm{Re}_\tau=u_\tau\delta/\nu$ and ν is the kinematic viscosity. The skin friction velocity is estimated at u_τ=0.0219 m/s by means of regression of $u^+=1/\kappa\ln y^+ + C$, where κ=0.41, C=5.0, between y^+=44 and y^+=200, and corresponds to a friction coefficient of C_f=0.00345. Please note that this paper has already made several appropriate additions and amendments when quoting existing excellent results from Schröder et al. [15]. The Kolmogorov dissipation scale η is the smallest scale of the multi-scale turbulent system, indicating the fluctuating kinetic energy at the action of molecular viscosity into thermal energy; Taylor differential scale λ is the length scale of the smallest scale eddies identifiable and produced in the turbulent flow.

In addition, the shear scale L_S is defined as the retroflex scale producing eddies owing to the role of the average velocity gradient in the shear turbulent flow field. When the largest scale is the order of magnitude of mean motions, we define integral scale as their characteristic scale. More details can be found in Yang et al. [16]. As we can see from Figure 2, the buffer layer (for wall-normal distance in wall

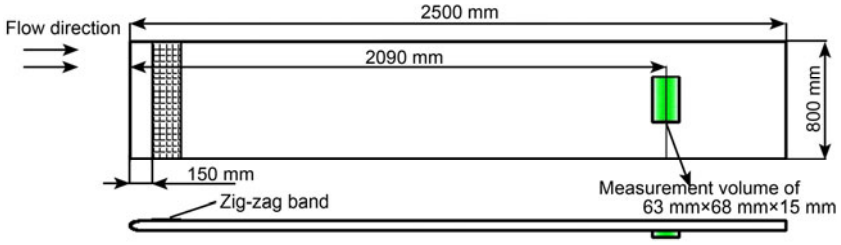

Figure 1 (Color online) Schematic diagram of the experimental plate and measurement volume parameters.

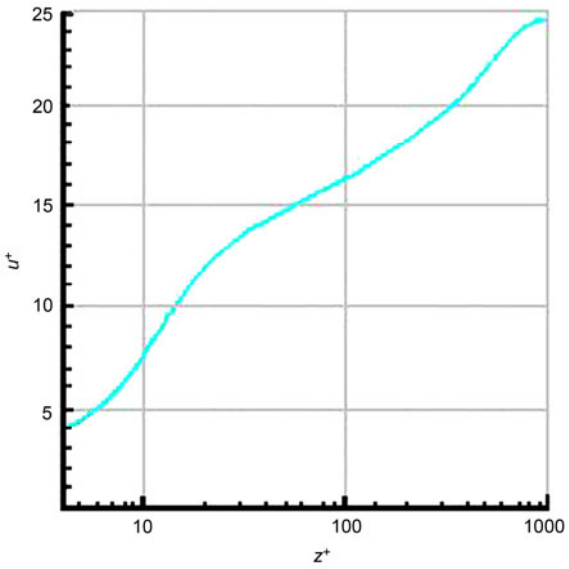

Figure 2 (Color online) Mean velocity profile of the TBL at Re_θ~2460 based on the momentum thickness. u^+ is the mean velocity normalized with viscous scales.

units z^+~13–28), log-layer (for $28<z^+<283$) and bulk region (for $z^+>283$) can be distinguished in the semi-log plot of the profile according to the characteristics of their respective curvature, although the linear viscous sub-layer region (for $z^+<10$) could not be resolved sufficiently.

The second step applied a high-repetition rate tomographic PIV system which was synchronized with a Programmable Timing Unit (LaVision PTU9) controlled by DaVis7.3 software by making use of a diode-pumped double-cavity Quantronix Nd: YLF laser, with a pulse energy of 25 mJ at 1 kHz, and six Photron CMOS cameras with 1024 pixels×1024 pixels in full-frame mode. A volume of about 63 mm×68 mm×15 mm=1.65δ×1.79δ×0.4δ=1380 WU×1490 WU×328 WU in the x- (streamwise), y- (spanwise) and z- (wall normal) directions, respectively, centered 2090 mm downstream of the plate leading edge was illuminated at 1 kHz frequency, which was at the same time the PIV sampling frequency. Five sequences of 2040 image volumes were captured during a period of 2 s. A volume self-calibration (when analyzed by local 3D cross-correlations, the particle image volume was 32×32×32 voxel interrogation box size and overlap rate of 50%) and the 3D-3C velocity vector field reconstruction of the particle image volumes (also with 32×32×32 voxel interrogation box size but 75% overlap rate) were successively performed by the same DaVis7.3 software. Eventually, a series of instantaneous three-dimensional velocity vector volumes over a grid of 92×99×22 measurement points located every 0.687 mm (~15 WU) in all directions in space for each time 2 ms increment were obtained after errors were estimated [15]. Due to the complexity of this experimental system and the large amount of work to estimate experimental errors, this paper does not give the specific error estimation process. However, more details can be found in ref. [15].

Table 1 Basic fluid mechanical properties of the TBL, as estimated by PIV

Reynolds number (Re_θ/Re_τ)	2460/800
Free-stream velocity (U)	530 mm/s
Friction coefficient (C_f)	0.00345
Friction velocity (u_τ)	21.9 mm/s
Boundary-layer thickness (δ)	38.1 mm
Kolmogorov length scales (η)	~3–5 WU
Shear scales (L_s)	~40–100 WU
Taylor micro-scales (λ)	~20–50 WU
Integral scales (L)	~4000 WU

2.2 Data analysis methods

For turbulent flows, the existence of multi-scale eddy structures has been verified by the increasing results [3,8,9] and the movement of the fluid particles in the TBL is restricted by such eddy structures, which leads to intermittency of turbulent flows [17]. Therefore, multitudes of analysis methods are proposed to analyze the turbulent signals that signify the multi-scale structures. One method is the wavelet analysis decomposing the analyzed signal in both the physical and the scale space by convoluting such a signal with a wavelet that is the compact-supported analytic function [18].

Additionally, a method based on the locally averaged velocity structure function proposed by Liu et al. [19] was used to take into account the multi-scale character of the turbulent structures. They conducted the experimental investigation in a wind tunnel and the following study by Liu et al. [20] verifies that the locally averaged velocity structure function is in agreement with the wavelet-coefficient structure function. Tang et al. [21] developed the locally averaged velocity structure function with various spatial scales to the 2D case when they analyze the 2D TR-PIV signals. Accordingly, in the present study, the locally averaged velocity structure function will be extended into a 3D case for the 3D-3C flow fields measured by tomographic TR-PIV. Hence, we can obtain the spatial local-averaged velocity strain which is convincingly in accordance with the concept of wavelet-coefficient when utilizing Harr wavelet transformation in the streamwise direction as:

$$\begin{aligned} a_{11} &= W_x^x(l,b) = \delta u_x(l,b_x) \\ &= \overline{u(x,y,z)}_{x\in[b_x,b_x+l]} - \overline{u(x,y,z)}_{x\in[b_x-l,b_x]}, \\ a_{21} &= W_x^y(l,b) = \delta v_x(l,b_y) \\ &= \overline{v(x,y,z)}_{x\in[b_y,b_y+l]} - \overline{v(x,y,z)}_{x\in[b_y-l,b_y]}, \\ a_{31} &= W_x^z(l,b) = \delta w_x(l,b_z) \\ &= \overline{w(x,y,z)}_{x\in[b_z,b_z+l]} - \overline{w(x,y,z)}_{x\in[b_z-l,b_z]}, \end{aligned} \tag{1}$$

where $W_x^x(l,b)$, $W_x^y(l,b)$ and $W_x^z(l,b)$ indicate respectively the streamwise ($-x$), spanwise ($-y$) and wall-normal ($-z$) wavelet-coefficients of wavelet transformation along the streamwise direction in a certain spatial turbulent scale l at a certain spatial location b. $\overline{u(x,y,z)}$ is the locally averaged streamwise velocity of the fluid motion in two adjacent eddies whose centers are respectively located at $b_x+l/2$ and $b_x-l/2$. Thus, the local-averaged streamwise velocity strain $\delta u_x(l, b_x)$ physically reveals the tensile and compressive deformation of certain structures in turbulent flows. Likewise the locally averaged spanwise velocity strain $\delta v_x(l, b_x)$ and wall-normal velocity strain $\delta w_x(l, b_x)$ are defined in eq. (1).

Similarly, the spatial local-averaged velocity strains in the spanwise and wall-normal directions can be defined as:

$$\begin{aligned}
a_{12} &= W_y^x(l,b) = \delta u_y(l,b_x) \\
&= \overline{u(x,y,z)}_{x\in[b_x,b_x+l]} - \overline{u(x,y,z)}_{x\in[b_x-l,b_x]}, \\
a_{22} &= W_y^y(l,b) = \delta v_y(l,b_y) \\
&= \overline{v(x,y,z)}_{x\in[b_y,b_y+l]} - \overline{v(x,y,z)}_{x\in[b_y-l,b_y]}, \\
a_{32} &= W_y^z(l,b) = \delta w_y(l,b_z) \\
&= \overline{w(x,y,z)}_{x\in[b_z,b_z+l]} - \overline{w(x,y,z)}_{x\in[b_z-l,b_z]},
\end{aligned} \tag{2}$$

$$\begin{aligned}
a_{31} &= W_z^x(l,b) = \delta u_z(l,b_x) \\
&= \overline{u(x,y,z)}_{x\in[b_x,b_x+l]} - \overline{u(x,y,z)}_{x\in[b_x-l,b_x]}, \\
a_{32} &= W_z^y(l,b) = \delta v_z(l,b_y) \\
&= \overline{v(x,y,z)}_{x\in[b_y,b_y+l]} - \overline{v(x,y,z)}_{x\in[b_y-l,b_y]}, \\
a_{33} &= W_z^z(l,b) = \delta w_z(l,b_z) \\
&= \overline{w(x,y,z)}_{x\in[b_z,b_z+l]} - \overline{w(x,y,z)}_{x\in[b_z-l,b_z]}.
\end{aligned} \tag{3}$$

In particular, these nine wavelet-coefficients in eqs. (1)–(3) physically imply the band-pass filtering of three velocity components in three directions in space, while such nine spatial local-averaged velocity strains actually demonstrate the velocity gradient tensor

$$\begin{pmatrix} \partial u/\partial x & \partial u/\partial y & \partial u/\partial z \\ \partial v/\partial x & \partial v/\partial y & \partial v/\partial z \\ \partial w/\partial x & \partial w/\partial y & \partial w/\partial z \end{pmatrix}, \text{ namely } \begin{pmatrix} a_{11} & a_{12} & a_{13} \\ a_{21} & a_{22} & a_{23} \\ a_{31} & a_{32} & a_{33} \end{pmatrix}.$$

There is a consensus that several certain relationships between coherent structures and burst (such as Q2 and Q4 events) do exist in the TBL. Accordingly, a new detection method (IQSM) of coherent structures can be illustrated as:

$$D(l,b) = \begin{cases} 1\ (\mathrm{Q}_2), & \text{if} \quad u'<0 \ \&\&\ a_{11}^-<0 \ \&\&\ a_{11}^+>0 \\ & \quad \&\&\ w'>0 \ \&\&\ a_{31}^->0 \ \&\&\ a_{31}^+<0, \\ -1\ (\mathrm{Q}_4) & \text{else if} \quad u'>0 \ \&\&\ a_{11}^->0 \ \&\&\ a_{11}^+<0 \\ & \quad \&\&\ w'<0 \ \&\&\ a_{31}^-<0 \ \&\&\ a_{31}^+>0, \\ 0 & \text{otherwise,} \end{cases} \tag{4}$$

where $D(l,b)$ is the detection function in certain turbulent scale l at certain location b, and $a_{11}^- = \delta u_x(l,b_x)^-$ is the left neighborhood value of streamwise local-averaged velocity strain at location b_x, while a_{11}^+ is the right neighborhood one. Eq. (4) physically shows that Q2 events arise when $u'<0$, $w'>0$ and u', w' reach the local minimum and maximum respectively while Q4 events take place in $u'>0$, $w'<0$ and u', w' reach the local extremums respectively, which largely contribute to the Reynolds shear stress [11, 12]. Similarly, Q1 event takes place at $u'>0$, $w'>0$ while Q3 event happens at $u'<0$, $w'<0$.

Considering the quasi-periodic repeatability [2] of burst events and the extended self-similarity of multi-scale eddy coherent structures, a new conditional sampling method based on the IQSM to extract turbulent coherent structures is given by

$$\left\langle f(l_j,x)\right\rangle_{Q_2} = \frac{1}{N_j}\sum_{i=1}^{N_j} f(b_i+x),\ x\in\left[-\frac{l_j}{2},\frac{l_j}{2}\right], \quad \text{while}: D(l_j,b_i)=1, \tag{5a}$$

$$\left\langle f(l_j,x)\right\rangle_{Q_4} = \frac{1}{N_j}\sum_{i=1}^{N_j} f(b_i+x),\ x\in\left[-\frac{l_j}{2},\frac{l_j}{2}\right], \quad \text{while}: D(l_j,b_i)=-1, \tag{5b}$$

where $\langle\ \rangle$ represents the ensemble average of certain variables, and $f(l_j, x)$ is the wondering conditional phase average component which respectively stands for fluctuating velocity, or fluctuating vorticity etc. investigated in this paper. N_j is the number of j-th scale of Q2 (ejection) and Q4 (sweep) events, while l_j represents the duration of j-th scale of coherent structures.

3 Results and discussion

The spatial local-averaged velocity strains with four scales were calculated according to eq. (1) along the streamwise direction by using the 3D-3C database of time series of velocity vector field measured by tomographic TR-PIV. Here we need to point out that only four-scale local-averaged velocity strains were obtained due to limits of insufficient data points in the wall-normal direction. Moreover, spatial phase average components, such as fluctuating velocity and fluctuating vorticity with four scales, were obtained by firstly extracting them in alignment-superimposed phase averaging several rectangular volumes of 33×33×9 (x×y×z) measurement points (namely of about 495×495×135 WU^3 or 0.59×0.59×0.16δ^3) whose centers are in the spatial locations where they meet the conditional eqs. (5a) and (5b), respectively. In other words, this also means that Q2 and Q4 bursting events are the centers of turbulent coherent structure spatial topology.

The three-level-value iso-surface contours of the streamwise fluctuating vorticity distribution for four scales are given in Figure 3 where the Q2 events happened in the centers. As can be seen in such figures, the similarity of multi-scale turbulent structures which the streamwise fluctuating vorticity (ω_1) represents clearly exist, especially between the third and fourth scale cases (see Figures 3(c) and 3(d)).

More specifically, there are a couple of counter-rotating quasi-streamwise vortices located on both sides of the Q2 event which look like two peanuts with an angle of around 45° between their necks and the virtual wall-bounded plane (here it is not the real flat-plate plane). In fact, such two reverse quasi-streamwise vortices extend toward the wall in the upstream flow field of Q2 events in the larger scale cases although they can only be partly seen because the potential turbulent structures are too large to be totally illustrated in the rectangular volume in the fourth scale. However, it is reasonable to speculate that such a couple of vortices will become streamwise when they are as close to the wall as possible, which is well in accordance with the hairpin vortex model proposed by Adrian [8].

In order to further study topologies of turbulent coherent structures in the spanwise and wall-normal direction, the three-level-value iso-surface contours of the spanwise and wall-normal fluctuating vorticity distributions (ω_2 and ω_3) for four scales are respectively showed in Figures 4 and 5. Here we consider that the first scale and the second scale are small-scale cases while the third and fourth scales are large-scale ones. Interestingly, a closer similarity comes to pass among small-scale spanwise coherent eddies while the behavior is the same among large-scale coherent structures. This may be explained by more interactions among different vortices, in the case that vortex catch-up and merger happen when they move downstream and grow up in the streamwise and spanwise directions respectively [22].

In comparison, the wall-normal turbulent structures that are illustrated by normal vorticity distributions shaped like a "butterfly" are identical among all scales. Therefore, in a word, there is a stronger similarity of coherent structures along the wall-normal direction while some slight difference appears between the small-scale and large-scale structures in the TBL along the streamwise and spanwise directions respectively. This phenomenon manifests that the streamwise and spanwise topological characters of coherent structures are greatly changed as vortex merger and catch-up takes place whereas they increase only in size along the wall-normal direction.

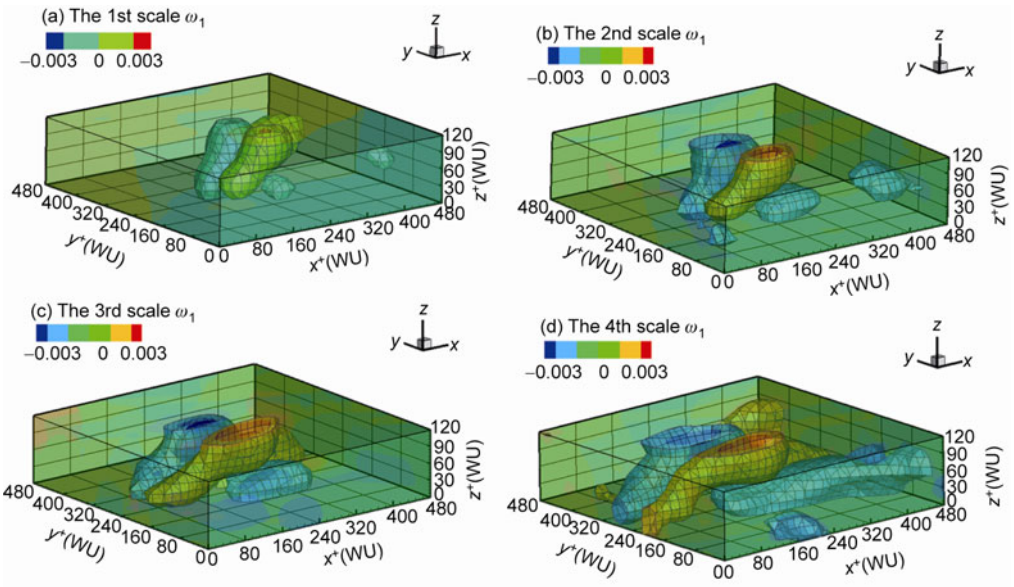

Figure 3 The three-level-value iso-surface contours of the streamwise fluctuating vorticity distribution for four scales, color coded by sign and strength. (a) The first scale; (b) the second scale; (c) the third scale; (d) the fourth scale.

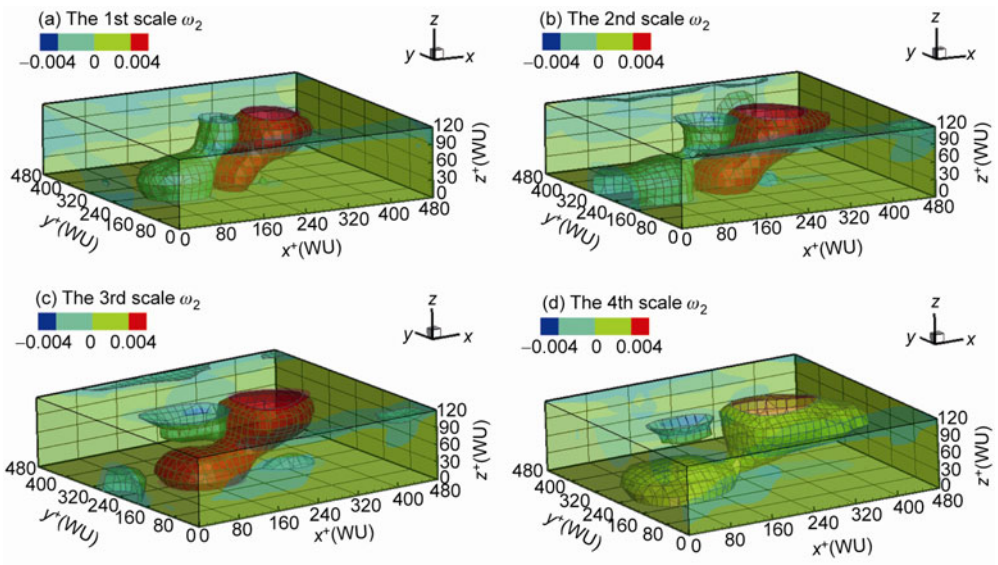

Figure 4 The three-level-value iso-surface contours of the spanwise fluctuating vorticity distributions for four scales, color coded by sign and strength. (a) The first scale; (b) the second scale; (c) the third scale; (d) the fourth scale.

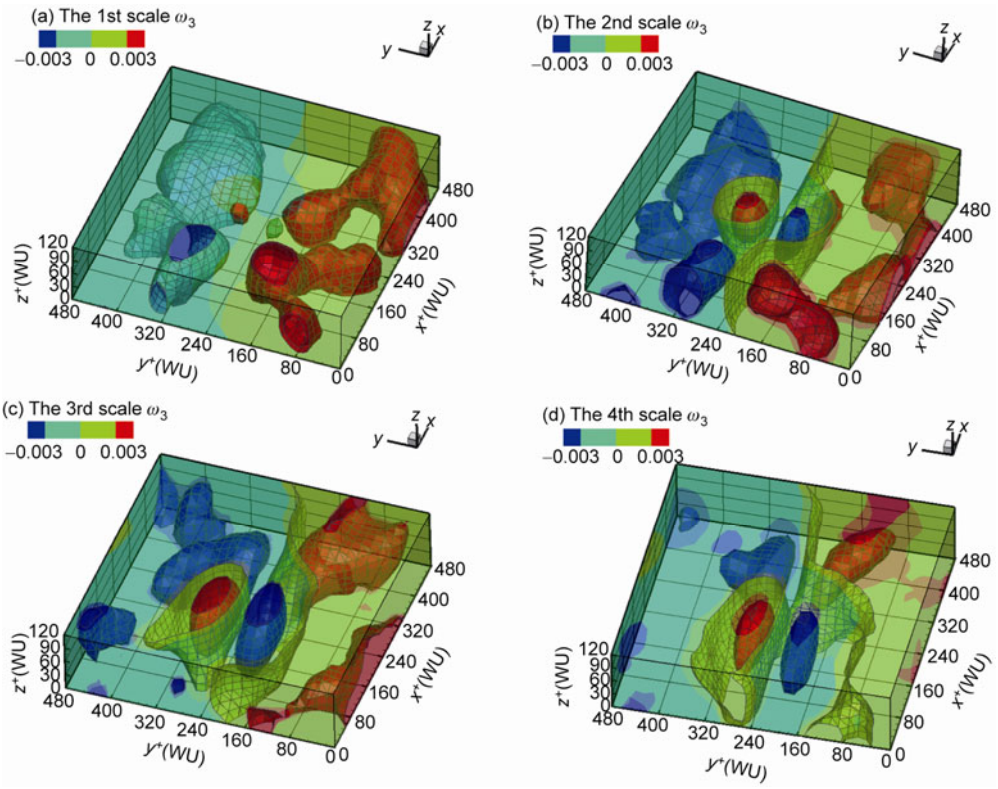

Figure 5 The three-level-value iso-surface contours of the wall-normal fluctuating vorticity distributions for four scales, color coded by sign and strength. (a) The first scale; (b) the second scale; (c) the third scale; (d) the fourth scale.

In order to avoid the interference of small-scale turbulent eddy structures in the large-scale ones, this paper is mainly concerned with large-scale structures. The small-large coherent structures will be analyzed later in other works unpublished. There is a blue colored region where its spanwise scale of the low-speed streak increases approximately from 300 WU to 360 WU as the wall-normal position increases for the fourth scale case illustrated in Figure 6(a). This is consistent with the average bursting period calculated by using the spatial auto-correlation function method along the spanwise direction at the same scale [16]. More specifically, the slice with tangent vectors in Figure 7 clearly demon-

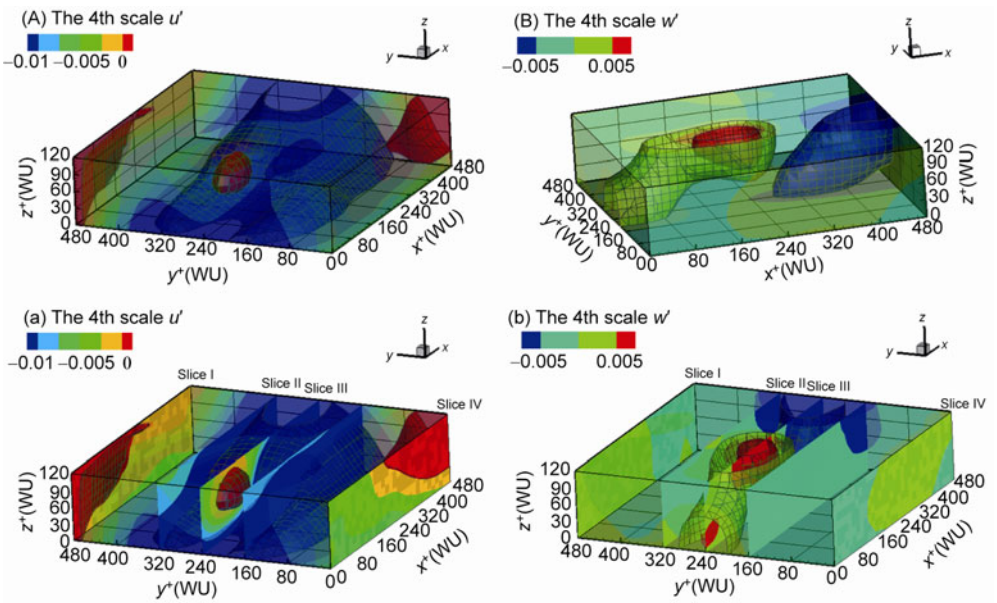

Figure 6 The streamwise (left) and wall-normal (right) fluctuating velocity distributions in the fourth scale, color coded by sign and strength. (A) (B) the iso-surface contours with three-level-values; (a) (b) the spanwise positions of four slices (I, II, III, IV).

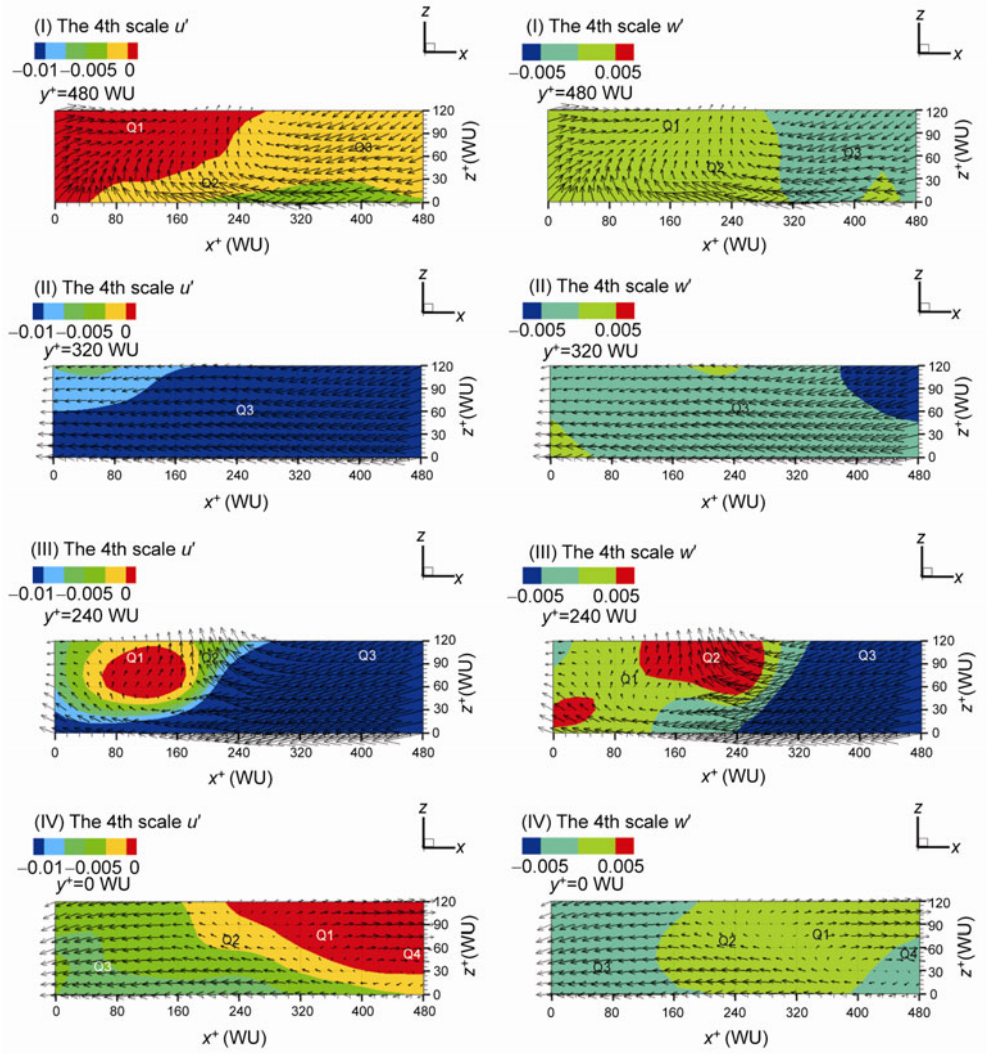

Figure 7 The four slices (I, II, III, IV) of streamwise (left) and wall-normal (right) velocity distributions with tangent velocity vectors in the positions marked in Figure 6, color coded by sign and strength.

strates the Q2 event as the center (corresponding detection center point x^+=240 WU, y^+= 240 WU, z^+=60 WU) surrounding a Q1 event upstream and a Q3 event downstream respectively in slice III. With traditional and classical views, it is the Q2 event that ejects the low-speed fluid away from the wall. However, this arises together with a Q1 event (see slices I and III) and contributes to the ejection process after a Q3 event (see slices II and III) of a long-time period, as well as a Q4 event (see slice IV) sweeping the high-speed fluid into the wall-plate, which fills the blank region so that the flow consistently satisfies the continuity conditions. In particular, there is a clot of high-speed fluid, upstream the Q2 event away from the wall with positive streamwise and wall-normal velocity, which looks like a head of certain coherent structure, such as a hairpin, to encounter a group of low-speed blue fluid in slice III. It might be one of the main characters of the Reynolds stress events. In brief, there is thereby a bursting continuous period along the streamwise direction in space of the downstream Q3 event, then Q2 lastly the upstream Q1 event in a typical bursting process (here referring to an ejection event). In fact, such an interesting bursting period arises from a typical sweep event showed in Figure 8. It is clear that the Q4 event arises following a Q1 event downstream, which together contributes to sweeping the high-speed fluid of wake region into the wall. Meanwhile a Q2 event that also can be seen in a lower normal position ejects outside the fluid of low-speed region near the wall although it fails on account of interactions with the upper high-speed fluid and then it becomes upstream the Q3 event. Most importantly, there is a singularity in mathematics labeled "S" in this figure near the center between the Q2 and Q4 events which seems like the stagnation point mentioned by Adrian [8]. The velocity vectors suddenly changed at the singularity where the Reynolds shear stress events intensively take place, particularly where the Q4 encountering the Q2 event, which greatly contributes to the momentum, energy and mass transforming. Accordingly, we believe that a possible bursting period order comes: Q4-S-Q2-Q3-Q2-Q1-Q4-S-Q2-Q3-Q2-Q1 if there is not a typical vortex with a core around it where Q2-Q1-Q4-Q1-Q2 or Q2-Q3-Q4-Q1-Q2 happens. Moreover, there is a higher probability of detecting ejections and a lower probability of detecting sweep events in each scale when we counted statistically, as listed in Table 2.

Lastly, for a clearer picture of the potential relation between vorticity and bursting events, the three-contour-slices with tangent velocity vectors of vorticity distributions referring to the Q2 event as the center are externalized in Figure 9 whose right parts are close-up slices at the middle positions where the detection center located with x^+=240 WU and y^+=240 WU respectively. A close-up slice of wall-normal vorticity at z^+=60 WU is specially given in Figure 10 to show how coherent structures develop and revolute along the spanwise direction when they move downstream. Specifically, the two counter-rotating quasi-streamwise vortices with reverse streamwise vorticity (see Figure 9 left-top part) are the main factors that enable the low-speed fluid near the wall to be lifted up by the Q2 or Q1 bursting event. Both increase in size and then downstream induce a couple of vortices smaller in size and lower in position but with an opposite sign that makes the fluid move towards the wall through the singularity (also labeled "S") that arises in a lower position of the ejection detection center. Similarly, the vortex showed by the spanwise vorticity also has the ability to induce another vortex upstream with reverse spanwise vorticity (see the bottom part of Figure 9). This vortex mutual induction mechanism [8,10,23] is the main factor in the turbulence production and maintenance.

As indicated in Figure 10, whether the Q2 event or Q4 as the center of detection, there are two pairs of vortices with opposite signs along the streamwise direction. Moreover, the vortices downstream are bigger than the ones upstream due to the mechanism of linear growth [23]. However, the singularity, which was mentioned before, labeled S here (see the right part of Figure 10 in the case of the sweep as the detection center) is the signature of nonlinear growth

Table 2 The number of ejection (Q2) and sweep (Q4) events in each scale

	1st scale	2nd scale	3rd scale	4th scale
Q2	236329	177978	123434	86862
Q4	209065	158629	109435	74558

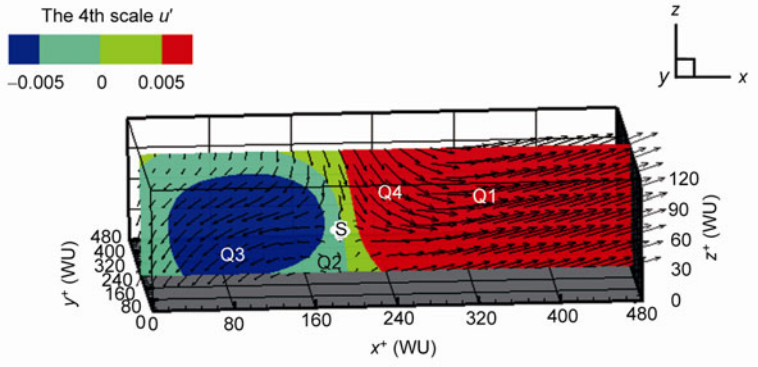

Figure 8 The slice of streamwise velocity distribution with tangent velocity vectors at y^+=240 WU containing a sweep event (Q4) as the center, color coded by sign and strength. Label S stands for singularity.

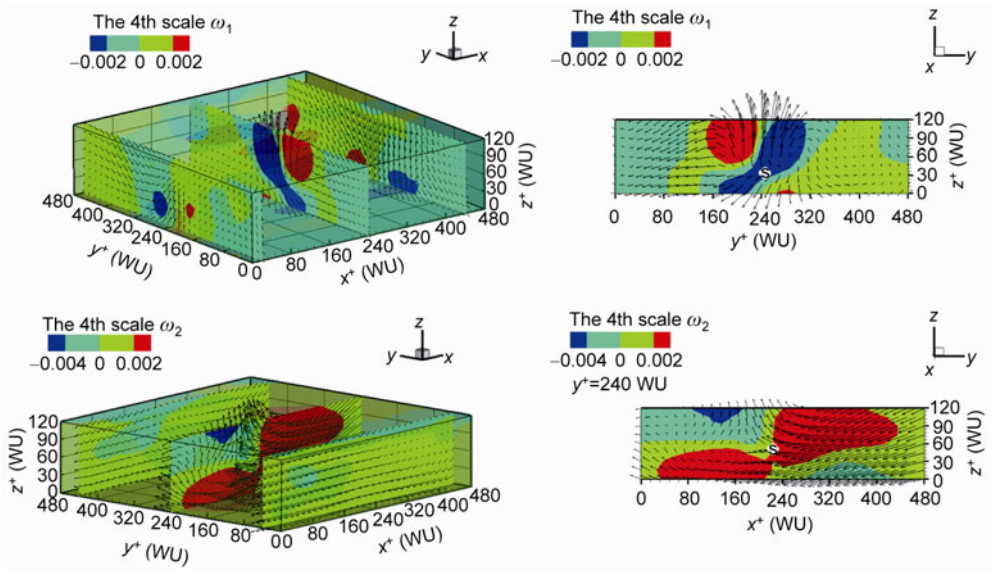

Figure 9 The three-contour-slices with tangent velocity vectors of streamwise (left-top) and spanwise(left-bottom) vorticity distributions and the close-up slice at middle positions (right), color coded by sign and strength.

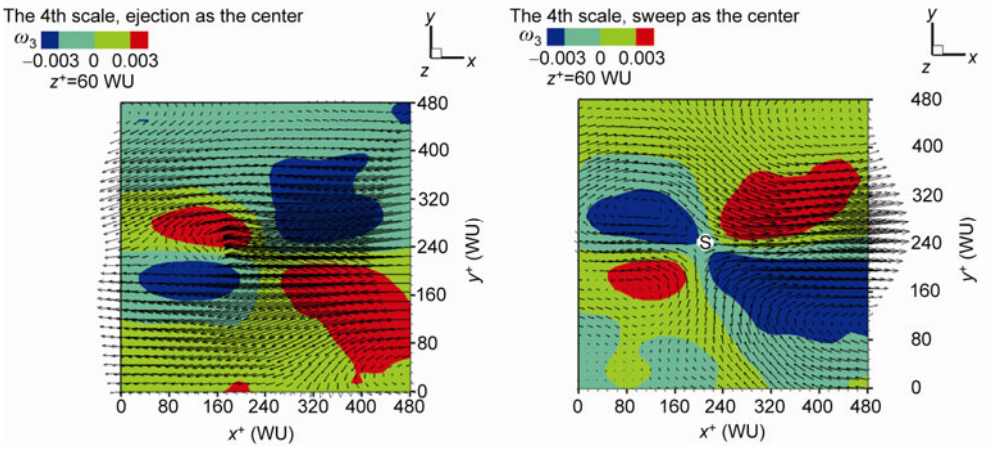

Figure 10 The close-up slice with tangent velocity vectors at z^+=60 WU, color coded by sign and strength of the wall-normal vorticity.

mechanism. Hence we believe that it is the instability of singularities which almost simultaneously appear together with typical Q2 or Q4 events that lead to the formation of such coherent structures in the TBL. Nevertheless, the physical meaning of the singularity that comes from mathematics needs further investigation in the future.

4 Conclusions

In this paper, the spatial local-averaged velocity strains with four scales were calculated along the streamwise direction based on the locally average velocity structure function by using the 3D-3C database of time series of velocity vector field measured by tomographic TR-PIV. Next, the spatial topologies of fluctuating velocity and fluctuating vorticity in the TBL with four scales were obtained by using the IQSM. Only large-scale structures, especially the fourth scale, were analyzed in order to avoid the interference of small-scale turbulent eddy structures in the large-scale ones.

To summarize, the similarity of multi-scale coherent structures do exist. However, the maximum similarity arises in the wall-normal direction. The streamwise and spanwise topological characters of coherent structures are greatly changed as the vortices merge and catch up with each other, whereas the vortices increase only in size at the wall-normal direction.

Furthermore, there is a region where its spanwise spatial scale of the low-speed streak increases from 300WU to 360 WU as the wall-normal position increases for the fourth scale, which agrees with the average bursting period calculated by using the spatial auto-correlation function method along the spanwise direction for the same scale. Besides, there is a couple of counter-rotating quasi-streamwise vor-

tices located on both sides of the Q2 event which extend toward the wall, parallel to the wall upstream but with an angle of around 45° between their necks and the virtual wall-bounded plane downstream.

Thirdly, the probability of the Q2 bursting event occurrence is slightly higher than that of the Q4 event occurrence when we counted statistically the number of ejection and sweep during detecting in each scale. And a possible bursting period order comes Q4-S-Q2-Q3-Q2-Q1-Q4-Q2-Q3-Q2-Q1 if there is not a typical vortex with a core around it where the order Q2-Q1-Q4-Q1-Q2 or Q2-Q3-Q4-Q1-Q2 cyclically happens, within which the Q2 event arises together with a Q1 event contributing to the ejection process that ejects the low-speed fluid far away from the wall while the Q4 event together with a Q3 event sweeps the high-speed fluid into the low-speed region near the wall.

Finally, coherent vortex structures, regardless of the streamwise vortices or the spanwise and wall-normal ones, all can upstream or downstream self-induce some new child-vortex structures through such an instable point called the singularity in mathematics that almost simultaneously appears together with typical Q2 or Q4 events. Presumably, such a kind of vortex mutual induction mechanism is the main factor in the production and maintenance of turbulence in wall bounded flows.

This work was supported by the National Basic Research Program of China (Grant No. 2012CB720101), the National Natural Science Foundation of China (Grant No. 10832001) and the Opening Subject of State Key Laboratory of Nonlinear Mechanics, Institute of Mechanics, Chinese Academy of Sciences. The authors are most grateful to the DLR Institute of Aerodynamics and Flow Technology for providing the tomographic TR-PIV database of time series of velocity vector field as well as the guidance and assistance of experimental technology for the present work.

1 Kline S J, Reynolds W C, Schraub F A, et al. The structure of turbulent boundary layers. J Fluid Mech, 1967, 30(4): 741–773
2 Robinson S K. Coherent motions in the turbulent boundary layer. Annu Rev Fluid Mech, 1991, 23(1): 601–639
3 Yang S Q, Jiang N. Wavelet analysis to detect multi-scale coherent eddy structures and intermittency in turbulent boundary layer. In: Proceedings of the eighth International Conference on Fuzzy Systems and Knowledge Discovery (FSKD'11). Shanghai: IEEE, 2011. 1241–1245
4 Cantwell B J. Organized motion in turbulent flow. Annu Rev Fluid Mech, 1981, 13(1): 457–515
5 Hussain A. Coherent structures and turbulence. J Fluid Mech, 1986, 173(1): 303–356
6 Theodorsen T. Mechanism of turbulence. In: Proceedings of the 2nd Midwestern Conference on Fluid Mechanics. Columbus, Ohio: Ohio State University, 1952. 1–18
7 Perry A E, Chong M S. On the mechanism of wall turbulence. J Fluid Mech, 1982, 119(1): 173–217
8 Adrian R J, Meinhart C D, Tomkins C D. Vortex organization in the outer region of the turbulent boundary layer. J Fluid Mech, 2000, 422(1): 1–54
9 Balakumar B J, Adrian R J. Large-and very-large-scale motions in channel and boundary-layer flows. Philos Trans R Soc Lond Ser A-Math Phys Eng Sci, 2007, 365(1852): 665–681
10 Panton R L. Overview of the self-sustaining mechanisms of wall turbulence. Prog Aerosp Sci, 2001, 37(4): 341–384
11 Elsinga G, Kuik D, Van Oudheusden B, et al. Investigation of the three-dimensional coherent structures in a turbulent boundary layer with Tomographic-PIV. In: Proceedings of 45th AIAA Aerospace Sciences Meeting and Exhibit. Reno, Nevada: AIAA, 2007. 1305
12 Lu S S, Willmarth W W. Measurements of the structure of the Reynolds stress in a turbulent boundary layer. J Fluid Mech, 1973, 60(3): 481–511
13 Sun K H, Shu W. On the burst detection techniques in wall-turbulence (in Chinese). Chin J Theor Appl Mech. 1994, 26(4): 488–493
14 Schröder A, Geisler R, Elsinga G E, et al. Investigation of a turbulent Spot and a tripped turbulent boundary layer flow using time-resolved tomographic PIV. Exp Fluids, 2008, 44(2): 305–316
15 Schröder A, Geisler R, Staack K, et al. Eulerian and Lagrangian views of a turbulent boundary layer flow using time-resolved tomographic PIV. Exp Fluids, 2011: 1–21
16 Yang S Q, Jiang N. On the measurement of spatial characteristic scale in turbulent boundary layer based on tomographic time-resolved PIV (in Chinese). J Exp Mech, 2011, 26(04): 369–376
17 Jiang N, Zhang J. Detecting multi-scale coherent eddy structures and intermittency in turbulent boundary layer by wavelet analysis. Chin Phys Lett, 2005, 22: 1968–1971
18 Farge M, Schneider K. Coherent Vortex Simulation (CVS), a semi-deterministic turbulence model using wavelets. Flow Turbul Combust, 2001, 66(4): 393–426
19 Liu W, Jiang N. Three kinds of velocity structure function in turbulent flows. Chin Phys Lett, 2004, 21: 1989–1992
20 Liu J H, Jiang N, Wang Z D, et al. Multi-scale coherent structures in turbulent boundary layer detected by locally averaged velocity structure functions. Appl Math Mech, 2005, 26(4): 495–504
21 Tang Z Q, Jiang N. TR PIV experimental investigation on bypass transition induced by a cylinder wake. Chin Phys Lett, 2011, 28: 054702
22 Tomkins C D, Adrian R J. Spanwise structure and scale growth in turbulent boundary layers. J Fluid Mech, 2003, 490: 37–74
23 Schoppa W, Hussain F. Coherent structure generation in near-wall turbulence. J Fluid Mech, 2002, 453: 57–108